JTE HCMUTE
ISSN: 2615-9740

JOURNAL OF TECHNICAL EDUCATION SCIENCE
Ho Chi Minh City University of Technology and Education
Website: https://jte.edu.vn
Email: jte@hcmute.edu.vn

Vibration of the Metal Foam Sandwich Plates With FG-CNTRC Face Sheets via Isogeometric Analysis

Duy-Khang Pham, Minh-Tan Huynh, Tan-Hung Pham*
Ho Chi Minh City University of Technology and Education, Vietnam

*Corresponding author. *Email: hungpht@hcmute.edu.vn*

ARTICLE INFO

Received: 23/04/2025
Revised: 13/05/2025
Accepted: 09/06/2025
Published online: 10/11/2025

KEYWORDS

Free vibration;
Isogeometric analysis (IGA);
Higher-order shear deformation theory;
Metal foam;
Carbon nanotube.

ABSTRACT

The objective of this paper is to investigate the free vibration behavior of sandwich plates composed of a metal foam core and two face sheets made of carbon nanotube-reinforced composite (CNTRC) materials. To achieve this, Reddy's higher-order shear deformation theory (HSDT) combined with the isogeometric approach (IGA) is employed to develop the numerical model. The equations of motion are systematically derived using Hamilton's principle, ensuring an accurate representation of both displacement and stress fields through the plate thickness. The proposed formulation is validated by comparing the present numerical results with available solutions reported in the existing literature, demonstrating excellent agreement. A comprehensive parametric study is conducted to assess the effects of key factors such as porosity distribution, CNT volume fraction, CNT distribution pattern, boundary conditions, and geometrical parameters on the natural frequencies of sandwich plates. The findings provide valuable insights for the optimal design and performance evaluation of advanced lightweight structural components with customized mechanical properties for aerospace, mechanical, and civil engineering applications.

Doi: https://doi.org/10.54644/jte.2025.1840

1. Introduction

Currently, researchers worldwide are highly interested in metal foam materials due to their outstanding properties. To simplify the analysis of vibration behavior, deflection, and instability, this material is often manufactured into structural forms such as beams, plates, and shells for analysis based on existing theories. For example, Chen et al. [1] employed the Ritz method to analyze the nonlinear free vibration of foam beams under shear deformation based on Timoshenko beam theory. Yan Qing Wang et al. [2] used the Chebyshev Collocation Method (CCM) to investigate the free vibration of sandwich beams with a metal foam core resting on a Winkler-Pasternak elastic foundation. Additionally, during the manufacturing process, voids were detected in metal foam plates, prompting many studies to analyze this issue. For instance, Barati et al. [3] analyzed the free vibration and stability of foam plates made of piezoelectric functionally graded materials based on a four-variable refined plate theory. Wattanasakulpong and Chaikittiratana [4] studied the bending vibration of beams made from functionally graded materials under various boundary conditions using Timoshenko beam theory and the Chebyshev grid point method. Ebrahimi et al. [5] investigated the vibration characteristics of the functionally graded (FG) magneto-electro-elastic plate. Furthermore, Wang et al. [6] analyzed the bending of three-dimensional graphene foam plates using a two-variable refined theory. Using higher-order shear deformation theory (HSDT), Mojahedin et al. [7] analyzed the nonlinear buckling of saturated circular metal foam plates with functionally graded properties, comparing their results with classical and first-order theories.

In recent years, CNTs (Carbon Nanotubes) have been widely and diversely applied across various industries. They are gradually replacing traditional materials due to their improved properties. For instance, Lei et al. [8] investigated and analyzed the free vibration of quadrilateral plates made of functionally graded composite materials reinforced with CNTs resting on a Pasternak foundation using the IMLS-Ritz method. On a similar topic, Zhang et al. [9] employed HSDT to study the displacement

fields of CNT-reinforced plates. Additionally, Jiao and collaborators [10] analyzed the dynamic bending behavior of CNT-reinforced composite cylindrical shells using a semi-analytical method.

The isogeometric analysis (IGA) method is a numerical computation technique that integrates geometric modeling with engineering analysis, particularly utilizing Non-Uniform Rational B-Splines (NURBS) basis functions to describe deformation fields in engineering analysis. For instance, Hughes et al. [11] introduced IGA to establish a strong link between Computer-Aided Design and finite element analysis (FEA). Additionally, Kacprzyk et al. [12] implemented IGA in the MATLAB environment, focusing on new element concepts and geometric data interpretation for future research applications. Since then, many researchers have successfully applied IGA to analyze structural components, including plates, shells, and beams. For instance, Huynh et al. [13] investigated the free vibration, stability, and bending of the FG curved beams with circular, elliptical, parabolic, and cycloid geometries using IGA. Furthermore, Thai et al. [14] employed IGA combined with a three-variable shear deformation theory to analyze the free vibration, static bending, and stability of multilayered composite plates.

To date, no studies have reported on free vibration analysis of sandwich plates with a porous metal core and CNTs-reinforced face sheets using IGA combined with HSDT. Therefore, this paper aims to contribute to scientific research by formulating a numerical model for sandwich plates, where the core is analyzed with three porosity distributions: uniform, symmetric, and asymmetric, while the face sheets are reinforced with four CNTs patterns: uniform, X-shaped, O-shaped, and A-shaped. By using the HSDT in conjunction with IGA, the proposed model eliminates shear correction factors, mitigates shear locking, and accurately captures deformation through the plate thickness. Additionally, this study investigates the effects of boundary conditions, geometric ratios, porosity levels in the metal foam core, and CNTs reinforcement patterns on the free vibration response of the sandwich plate. The obtained numerical results serve as a valuable reference for future research and play a crucial role in the structural design of sandwich plates for various industrial applications.

2. The material properties

The sandwich plate's length and width are denoted as a and b, respectively. Additionally, h, h_c, h_f correspond to the thicknesses of the entire sandwich plate, core layer, and the face sheets, respectively, as depicted in Figure 1a. Figures 1b, 1c, and 1d demonstrate uniform (P-I), symmetric (P-II), and asymmetric (P-III) distributions of the metal foam material. The reinforcement materials on the face sheets of the sandwich plate is distributed in four patterns, namely: uniform (FG-UD), X-shaped (FG-UX), O-shaped (FG-UO), and A- shaped (FG-UA). The CNTs distributions are presented in Figure 2.

2.1. Porous metal foam core

The metal foam material is considered with three characteristic distributions, as shown in Figure 1 for analysis and evaluation. The characteristic parameters, such as the elastic modulus (E), shear modulus (G), and density, are presented as follows [15]

Uniform porosity distribution (P-I):

$$E^c = E_1\left(1-e_0\xi\right);\ G^c = G_1\left(1-e_0\xi\right);\ \rho^c = \rho_1\left(1-\sqrt{1-e_0\xi}\right)$$

Symmetric porosity distribution (P-II):

$$E^c = E_1\left[1-e_0\cos\left(\frac{\pi z}{h}\right)\right];\ G^c = G_1\left[1-e_0\cos\left(\frac{\pi z}{h}\right)\right];\ \rho^c = \rho_1\left[1-e_m\cos\left(\frac{\pi h}{h}\right)\right] \quad (1)$$

Asymmetric porosity distribution (P-III):

$$E^c = E_1\left[1-e_0\cos\left(\frac{\pi z}{2h}+\frac{\pi}{4}\right)\right];G^c = G_1\left[1-e_0\cos\left(\frac{\pi z}{2h}+\frac{\pi}{4}\right)\right];\rho^c = \rho_1\left[1-e_m\cos\left(\frac{\pi h}{h}+\frac{\pi}{4}\right)\right]$$

where G_1, E_1, and ρ_1 are defined as the maximum shear modulus, elastic modulus, and density, respectively.

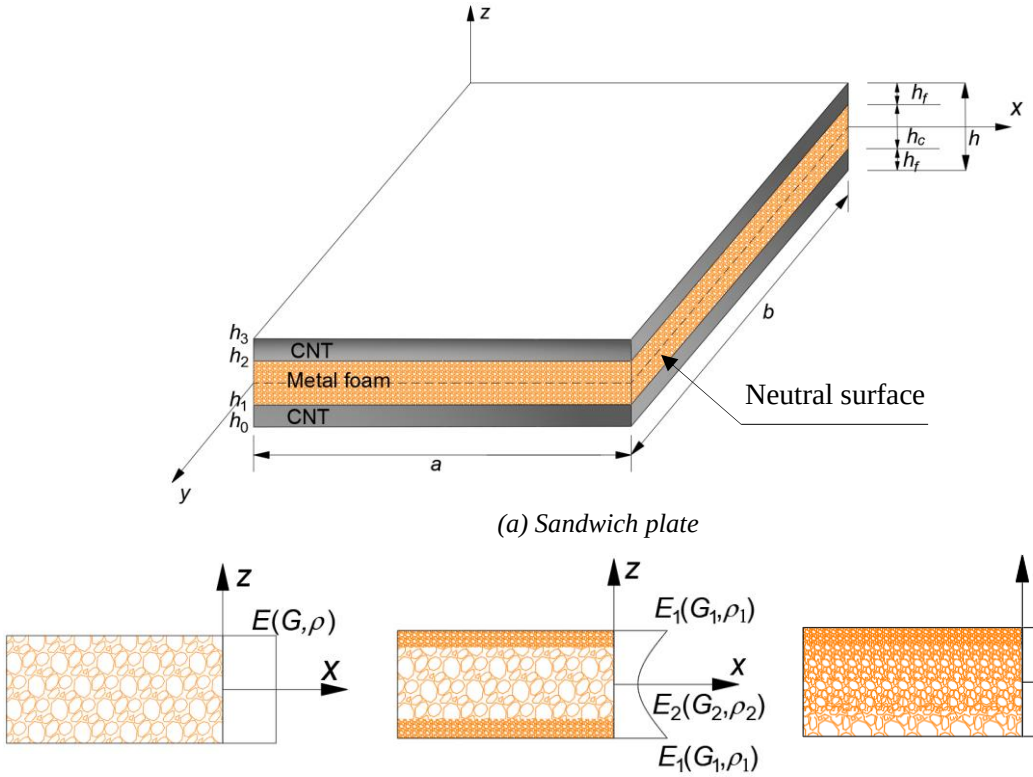

(a) Sandwich plate

(b) Uniform porosity (P-I) *(c) Symmetric porosity (P-II)* *(d) Asymmetric porosity (P-III)*

Figure 1. *Geometric configuration of the sandwich plate with three different metal foam distribution type: (a) Sandwich plate, (b) P-I, (c) P-II, (d) P-III.*

Additionally, e_0 and e_m are defined as the porosity and mass porosity coefficients, respectively.

$$e_0 = 1 - \frac{E_2}{E_1} = 1 - \frac{G_2}{G_1}, 0 < e_0 < 1;\ e_m = 1 - \frac{\rho_2}{\rho_1}, 0 < e_m < 1 \tag{2}$$

where G_2, E_2, and ρ_2 represent the minimum shear modulus, elastic modulus, and density, respectively.

The coefficient ξ in Eq. (1) is defined as follows [15]

$$\xi = \frac{1}{e_0} - \frac{1}{e_0}\left(\frac{2}{\pi}\sqrt{1-e_0} - \frac{2}{\pi} + 1\right)^2 \tag{3}$$

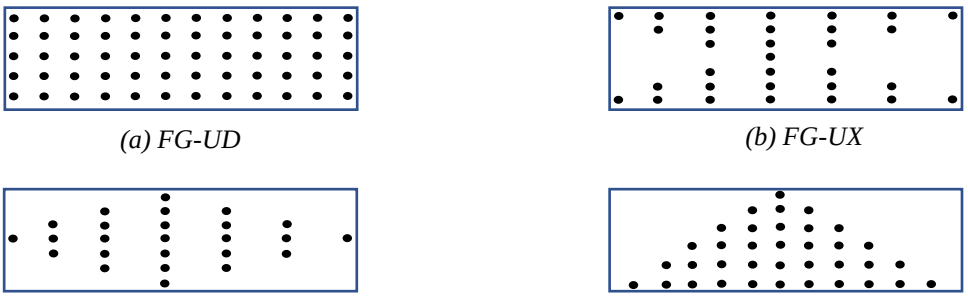

(a) FG-UD *(b) FG-UX*

(c) FG-UO *(d) FG-UA*

Figure 2. *The CNTs distributions: (a) FG-UD, (b) FG-UX, (c) FG-UO, (d) FG-UA.*

JTE HCMUTE
ISSN: 2615-9740
JOURNAL OF TECHNICAL EDUCATION SCIENCE
Ho Chi Minh City University of Technology and Education
Website: https://jte.edu.vn
Email: jte@hcmute.edu.vn

2.2. FG-CNTRC face sheets

According to the study, FG-CNTRC materials made of a matrix material embedded with CNTs, as illustrated in Figure 2. The volume fractions of CNTs for different CNTs distribution patterns are presented as follows [16]-[19]

$$\begin{aligned}
&\text{FG-UD} && V_{CNT} = \hat{V}_{CNT} && \\
&\text{FG-UA} && V_{CNT}(z) = \begin{cases} 2\left(\dfrac{h_2 - z}{h_2 - h_3}\right)\hat{V}_{CNT} & \text{Top surface} \\ 2\left(\dfrac{z - h_1}{h_0 - h_1}\right)\hat{V}_{CNT} & \text{Bottom surface} \end{cases} && \\
&\text{FG-UX} && V_{CNT}(z) = \begin{cases} 2\left(\left|\dfrac{h_2 + h_3 - 2z}{h_2 - h_3}\right|\right)\hat{V}_{CNT} & \text{Top surface} \\ 2\left(\left|\dfrac{h_0 + h_1 - 2z}{h_0 - h_1}\right|\right)\hat{V}_{CNT} & \text{Bottom surface} \end{cases} && (4) \\
&\text{FG-UO} && V_{CNT}(z) = \begin{cases} 2\left(1 - \left|\dfrac{h_3 + h_2 - 2z}{h_2 - h_3}\right|\right)\hat{V}_{CNT} & \text{Top surface} \\ 2\left(1 - \left|\dfrac{h_0 + h_1 - 2z}{h_0 - h_1}\right|\right)\hat{V}_{CNT} & \text{Bottom surface} \end{cases} &&
\end{aligned}$$

where

$$\hat{V}_{CNT} = \frac{\rho_m w_{CNT}}{\rho_{CNT}(1 - w_{CNT}) + \rho_m w_{CNT}} \tag{5}$$

where ρ_m and ρ_{CNT} are the densities of the matrix and CNTs, respectively, w_{CNT} represents the mass fraction of CNTs.

The material properties of FG-CNTRC are characterized by the following formulas [20]-[22]

$$\begin{aligned}
&E_{11}^f = \eta_1 V_{CNT} E_{11}^{CNT} + V_m E^m;\ E_{22}^f = \frac{\eta_2}{V_{CNT}/E_{22}^{CNT} + V_m/E^m};\ G_{12}^f = \frac{\eta_3}{V_{CNT}/G_{12}^{CNT} + V_m/G^m} \\
&\nu_{12}^f = V_{CNT}\nu_{12}^{CNT} + V_m\nu_m;\ \nu_{21}^f = E_{22}/E_{11}\nu_{12}^{CNT};\ \rho^f = V_{CNT}\rho_{CNT} + V_m\rho_m;\ V_m = 1 - V_{CNT}
\end{aligned} \tag{6}$$

where G_m and G_{12}^{CNT} respectively indicate the shear moduli of the matrix and CNTs, while E_{11}^{CNT} and E_{22}^{CNT} refer to the CNTs elastic modulus, E^m is the matrix's elastic modulus. Additionally, ν_m and ν_{12}^{CNT} are the Poisson's ratios of the matrix and CNTs, respectively. The parameters η_1, η_2, and η_3 are the efficiency parameters, which are presented in Table 1.

Table 1. *Efficiency parameters of CNTs for different volume fractions corresponding to each CNTs volume fraction [20].*

$\hat{V}_{CNT}$	η_1	η_2	η_3
0.11	0.149	0.934	0.934
0.14	0.150	0.941	0.941
0.17	0.149	1.381	1.381

The material characteristics of FG-CNTRC include the following [23]

$$E_{11}^{CNT}=5646.6\text{GPa};E_{22}^{CNT}=7080\text{GPa};G_{12}^{CNT}=1944.5\text{GPa};\nu_{12}^{CNT}=0.175;\rho_{CNT}=1400\text{kg/m}^3;\\ E_m=2.1\text{GPa};\nu_m=0.34 \tag{7}$$

3. The basic equations

3.1. The higher-order shear deformation theory

Applying the HSDT [24], the strain field at any arbitrary point of the sandwich plate is expressed as follows

$$\mathbf{u}=\mathbf{u}_0+z\mathbf{u}_1+f\left(z\right)\mathbf{u}_2$$

$$\text{where }\mathbf{u}=\begin{Bmatrix}u\\v\\w\end{Bmatrix};\mathbf{u}_0=\begin{Bmatrix}u_0\\v_0\\w_0\end{Bmatrix};\mathbf{u}_1=\begin{Bmatrix}-w_{0,x}\\-w_{0,y}\\0\end{Bmatrix};\mathbf{u}_2=\begin{Bmatrix}\theta_x\\\theta_y\\0\end{Bmatrix};\ f\left(z\right)=z-4z^3/3h^2 \tag{8}$$

where u_0, v_0 and w_0 are the displacement components in the x, y and z directions, respectively; θ_x and θ_y are defined as the rotations about the y and x axes, respectively; the notations '$,x$' and '$,y$' represent the partial derivatives of the functions with respect to x and y, respectively.

The strain tensor is determined as follows

$$\boldsymbol{\varepsilon}=\left\{\boldsymbol{\varepsilon}_b\quad\boldsymbol{\varepsilon}_s\right\}^T;\boldsymbol{\varepsilon}_b=\boldsymbol{\varepsilon}_{b0}+z\boldsymbol{\varepsilon}_{b1}+f\left(z\right)\boldsymbol{\varepsilon}_{b2};\boldsymbol{\varepsilon}_s=f'\left(z\right)\boldsymbol{\gamma}_s \tag{9}$$

where

$$\boldsymbol{\varepsilon}_{b0}=\begin{Bmatrix}u_{0,x}\\v_{0,y}\\u_{0,y}+v_{0,x}\end{Bmatrix};\boldsymbol{\varepsilon}_{b1}=-\begin{Bmatrix}w_{0,xx}\\w_{0,yy}\\2w_{0,xy}\end{Bmatrix};\boldsymbol{\varepsilon}_{b2}=\begin{Bmatrix}\theta_{x,x}\\\theta_{y,y}\\2\theta_{x,y}\end{Bmatrix};\boldsymbol{\gamma}_s=\begin{Bmatrix}\theta_x\\\theta_y\end{Bmatrix} \tag{10}$$

The stress-strain relationship equations are formulated based on Hooke's law as follows

$$\boldsymbol{\sigma}_b^{f,c}=\mathbf{C}_b^{f,c}\boldsymbol{\varepsilon}_b;\boldsymbol{\sigma}_s^{f,c}=\mathbf{C}_s^{f,c}\boldsymbol{\varepsilon}_s \tag{11}$$

where

$$\boldsymbol{\sigma}_b^{f,c}=\begin{Bmatrix}\sigma_x^{f,c}\\\sigma_y^{f,c}\\\tau_{xy}^{f,c}\end{Bmatrix};\mathbf{C}_b^f=\begin{bmatrix}\mathrm{C}_{11}^{f,c}&\mathrm{C}_{12}^{f,c}&0\\\mathrm{C}_{21}^{f,c}&\mathrm{C}_{22}^{f}&0\\0&0&\mathrm{C}_{66}^{f,c}\end{bmatrix};\ \boldsymbol{\sigma}_s^{f,c}=\begin{Bmatrix}\tau_{xz}^{f,c}\\\tau_{yz}^{f,c}\end{Bmatrix};\mathbf{C}_s^{f,c}=\begin{bmatrix}\mathrm{C}_{55}^{f,c}&0\\0&\mathrm{C}_{44}^{f,c}\end{bmatrix}$$

$$C_{11}^f=\frac{E_{11}}{\left(1-\nu_{12}\nu_{21}\right)};C_{12}^f=\frac{E_{11}\nu_{21}}{\left(1-\nu_{12}\nu_{21}\right)};C_{22}^f=\frac{E_{22}}{\left(1-\nu_{12}\nu_{21}\right)};C_{66}^f=G_{12};C_{55}^f=G_{12};C_{44}^f=G_{12} \tag{12}$$

$$C_{11}^c=C_{22}^c=\frac{E}{\left(1-\nu^2\right)};C_{12}^c=C_{21}^c=\frac{E}{\left(1-\nu^2\right)};C_{44}^c=C_{55}^c=C_{66}^c=G^c=\frac{E}{2\left(1+\nu\right)}$$

3.2. Variational principle

According to Hamilton's principle, the governing equation can be presented as follow

$$\int_0^t\left(\delta U+\delta K\right)\mathrm{d}t=0 \tag{13}$$

where δU and δK are the variations of elastic strain energy and kinetic energy, respectively.

$$\delta U = \int_\Omega \delta \bar{\boldsymbol{\varepsilon}}_b^T \mathbf{D}_b \bar{\boldsymbol{\varepsilon}}_b \mathrm{d}\Omega + \int_\Omega \delta \boldsymbol{\gamma}_s^T \mathbf{D}_s \boldsymbol{\gamma}_s \mathrm{d}\Omega \tag{14}$$

in which

$$\mathbf{D}_b = \begin{bmatrix} \mathbf{A}_u & \mathbf{B}_u & \mathbf{E}_u \\ \mathbf{B}_u & \mathbf{D}_u & \mathbf{F}_u \\ \mathbf{E}_u & \mathbf{F}_u & \mathbf{H}_u \end{bmatrix};\ \bar{\boldsymbol{\varepsilon}}_b = \left\{ \boldsymbol{\varepsilon}_{b0} \quad \boldsymbol{\varepsilon}_{b1} \quad \boldsymbol{\varepsilon}_{b2} \right\}^T$$

$$\begin{aligned} &\left(\mathbf{A}_u, \mathbf{B}_u, \mathbf{D}_u, \mathbf{E}_u, \mathbf{F}_u, \mathbf{H}_u\right) = \\ &\int_{-h/2}^{-h_c/2} \left(1, z, z^2, f(z), zf, f^2\right) \mathbf{C}_b^f \mathrm{d}z + \int_{-h_c/2}^{h_c/2} \left(1, z, z^2, f, zf, f^2\right) \mathbf{C}_b^c \mathrm{d}z + \int_{h_c/2}^{h/2} \left(1, z, z^2, f, zf, f^2\right) \mathbf{C}_b^f \mathrm{d}z \end{aligned} \tag{15}$$

$$\mathbf{D}_s = \int_{-h/2}^{-h_c/2} f'^2 \mathbf{C}_s^f \mathrm{d}z + \int_{-h_c/2}^{h_c/2} f'^2 \mathbf{C}_s^c \mathrm{d}z + \int_{h_c/2}^{h/2} f'^2 \mathbf{C}_s^f \mathrm{d}z$$

Additionally, the virtual kinetic energy is expressed as follows

$$\delta K = \int_V \delta \mathbf{u}^T \rho(z) \ddot{\mathbf{u}} \mathrm{d}V = \int_\Omega \delta \bar{\mathbf{u}}^T \mathbf{I}_m \ddot{\bar{\mathbf{u}}} \mathrm{d}\Omega \tag{16}$$

where V and Ω are the volume and the middle surface area of the plate, respectively. And

$$\begin{aligned} &\bar{\mathbf{u}} = \begin{Bmatrix} \mathbf{u}_0 \\ \mathbf{u}_1 \\ \mathbf{u}_2 \end{Bmatrix}; \mathbf{I}_\mathrm{m} = \begin{bmatrix} \mathbf{I}_0 & 0 & 0 \\ 0 & \mathbf{I}_0 & 0 \\ 0 & 0 & \mathbf{I}_0 \end{bmatrix}; \mathbf{I}_0 = \begin{bmatrix} I_1 & I_2 & I_4 \\ I_2 & I_3 & I_5 \\ I_4 & I_5 & I_6 \end{bmatrix} \\ &\left(I_1, I_2, I_3, I_4, I_5, I_6\right) = \\ &\int_{-h/2}^{-h_c/2} \rho^f \left(1, z, z^2, f, zf, f^2\right) \mathrm{d}z + \int_{-h_c/2}^{h_c/2} \rho^c \left(1, z, z^2, f, zf, f^2\right) \mathrm{d}z + \int_{h_c/2}^{h/2} \rho^f \left(1, z, z^2, f, zf, f^2\right) \mathrm{d}z \end{aligned} \tag{17}$$

The formulas in Eqs. (14) and (16), when substituted into Eq. (13), yield the weak form of the sandwich plate as follows

$$\int_\Omega \delta \bar{\boldsymbol{\varepsilon}}_b^T \mathbf{D}_b \bar{\boldsymbol{\varepsilon}}_b \mathrm{d}\Omega + \int_\Omega \delta \boldsymbol{\gamma}_s^T \mathbf{D}_s \boldsymbol{\gamma}_s \mathrm{d}\Omega + \int_\Omega \delta \bar{\mathbf{u}}^T \mathbf{I}_m \ddot{\bar{\mathbf{u}}} \mathrm{d}\Omega = 0 \tag{18}$$

3.3. Isogeometric approach

By using the NURBs basic function reported in ref. [11], the sets of displacements are approximated in the following form

$$\mathbf{u}^h(\eta, \zeta) = \sum_{i=1}^{m \times n} \mathbf{N}_i(\eta, \zeta) \mathbf{d}_i \tag{19}$$

where

$$\mathbf{N}_i(\eta, \zeta) = \mathbf{I}_{5\times5} N_i(\eta, \zeta);\ \mathbf{d}_i = \left\{ u_{0i} \quad v_{0i} \quad w_{0i} \quad \theta_{xi} \quad \theta_{yi} \right\}^T \tag{20}$$

where N_i and $\mathbf{d}_i$ are the NURBS shape functions and displacement vector, respectively; $\mathbf{I}_{5\times5}$ is 5×5 identity matrix.

By substituting the Eq. (19) into Eq. (10) , we obtain

$$\bar{\boldsymbol{\varepsilon}}_b = \sum_{i=1}^{m \times n} \left\{ \mathbf{B}_{b0i} \quad \mathbf{B}_{b1i} \quad \mathbf{B}_{b2i} \right\}^T \mathbf{d}_i = \sum_{i=1}^{m \times n} \mathbf{B}_{bi} \mathbf{d}_i; \boldsymbol{\gamma}_s = \sum_{i=1}^{m \times n} \mathbf{B}_{si} \mathbf{d}_i \tag{21}$$

with

$$\mathbf{B}_{b0i}=\begin{bmatrix} N_{i,x} & 0 & 0 & 0 & 0 \\ 0 & N_{i,y} & 0 & 0 & 0 \\ N_{i,y} & N_{i,x} & 0 & 0 & 0 \end{bmatrix};\mathbf{B}_{b1i}=-\begin{bmatrix} 0 & 0 & N_{i,xx} & 0 & 0 \\ 0 & 0 & N_{i,yy} & 0 & 0 \\ 0 & 0 & 2N_{i,xy} & 0 & 0 \end{bmatrix};\mathbf{B}_{b2i}=\begin{bmatrix} 0 & 0 & 0 & N_{i,x} & 0 \\ 0 & 0 & 0 & 0 & N_{i,y} \\ 0 & 0 & 0 & 2N_{i,y} & 0 \end{bmatrix} \tag{22}$$

$$\mathbf{B}_{si}=\begin{bmatrix} 0 & 0 & 0 & N_i & 0 \\ 0 & 0 & 0 & 0 & N_i \end{bmatrix}$$

Furthermore, the vector $\bar{\mathbf{u}}$ is reformulated according to Eq. (19) as follows

$$\bar{\mathbf{u}}=\{\mathbf{u}_0 \quad \mathbf{u}_1 \quad \mathbf{u}_2\}^T=\sum_{i=1}^{m\times n}\{\mathbf{N}_{0i} \quad \mathbf{N}_{1i} \quad \mathbf{N}_{2i}\}^T\mathbf{d}_i=\sum_{i=1}^{m\times n}\mathbf{N}_i\mathbf{d}_i \tag{23}$$

in which

$$\mathbf{N}_{0i}=\begin{bmatrix} N_i & 0 & 0 & 0 & 0 \\ 0 & N_i & 0 & 0 & 0 \\ 0 & 0 & N_i & 0 & 0 \end{bmatrix};\mathbf{N}_{1i}=\begin{bmatrix} 0 & 0 & -N_{i,x} & 0 & 0 \\ 0 & 0 & -N_{i,y} & 0 & 0 \\ 0 & 0 & 0 & 0 & 0 \end{bmatrix};\mathbf{N}_{2i}=\begin{bmatrix} 0 & 0 & 0 & N_i & 0 \\ 0 & 0 & 0 & 0 & N_i \\ 0 & 0 & 0 & 0 & 0 \end{bmatrix} \tag{24}$$

Substituting Eqs. (21) and (23) into Eq. (18), the weak form of the free vibration of the sandwich plate is expressed as follows

$$\left(\mathbf{K}-\omega^2\mathbf{M}\right)\underline{\mathbf{d}}=0 \text{ with } \mathbf{d}=\underline{\mathbf{d}}e^{i\omega t} \tag{25}$$

where ω and $\underline{\mathbf{d}}$ are defined as the natural frequency and mode shape, respectively. The matrices **K** and **M** are defined as follows

$$\mathbf{K}=\int_\Omega \mathbf{B}_b^T\mathbf{D}_b\mathbf{B}_b d\Omega+\int_\Omega \mathbf{B}_s^T\mathbf{D}_s\mathbf{B}_s d\Omega;\ \mathbf{M}=\int_\Omega \mathbf{N}_i^T\mathbf{I}_m\mathbf{N}_i d\Omega \tag{26}$$

4. Numerical results

In this section, a sandwich plate made of metal foam material and reinforced with two face sheets of carbon nanotube material is investigated under different boundary conditions (BCs). The boundary conditions applied to the sandwich plate include simply supported on all four edges (SSSS), clamped on all four edges (CCCC), simply supported on two edges and free on the remaining two edges (SFSF), and simply supported on two edges with clamped conditions on the other two edges (SCSC). These boundary conditions are described Eq. (27). In Eq. (27), applying the Dirichlet boundary conditions for the variables u_0, v_0, w_0, θ_x, and θ_y in the traditional FEM is relatively straightforward. For the essential boundary condition on the normal derivative $w_{0,n}$, the deflection w_0 is constrained to zero at the control points located adjacent to the boundary, as demonstrated in Figure 3 and according to the method proposed in [25].

SSSS $$\left(v_0,w_0,\theta_y\right)\Big|_{x=0,a}=0;\left(u_0,w_0,\theta_x\right)\Big|_{y=0,b}=0$$

SFSF $$\left(v_0,w_0,\theta_y\right)\Big|_{x=0,a}=0$$

SCSC $$\left(v_0,w_0,\theta_y\right)\Big|_{x=0,a}=0;\ \left(u_0,v_0,w_0,\theta_x,\theta_y,w_{0,n}\right)\Big|_{y=0,b}=0$$

CCCC $$\left(u_0,v_0,w_0,\theta_x,\theta_y,w_{0,n}\right)\Big|_{x=0,a}=0;\left(u_0,v_0,w_0,\theta_x,\theta_y,w_{0,n}\right)\Big|_{y=0,b}=0$$ (27)

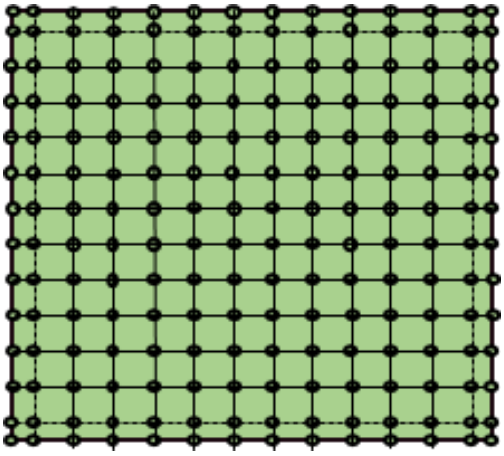

Figure 3. *The sandwich plate with 11×11 cubic elements.*

4.1. Comparison of Results

To verify the accuracy of the proposed approach, the vibration of the porous plate (h_f = 0) with different porosity distribution patterns is considered: P-I, P-II, and P-III. The material properties of the metal foam are taken as follows: E_1= 200 GPa, ν_1= 0.33, ρ_1= 7850 kg/m^3 from references [26], [27]. Different meshes, consisting of cubic elements with sizes 7×7, 9×9, 11×11, 13×13 and 15×15, are used. The polynomial degree is selected as $p = q = 3$. Table 2 provides the comparison results for the non-dimensional frequency $\varpi = \omega h\sqrt{\rho_1/E_1}$ of the metal foam plate under SSSS boundaries. The computer results obtained exhibit excellent agreement with the semi-analytical method, with reference solutions taken from [26]. Notably, the numerical results from different mesh divisions are identical. Therefore, the mesh with 11×11 elements is selected for further numerical computations. In addition, the lowest four normalized natural frequencies $\bar{\Omega} = 100\omega h\sqrt{\rho_1/E_1}$ of the porous plate under different porosity distributions and width to length ratios are presented in Table 3. The material properties E_1, ρ_1, and ν_1 are adopted from reference [27]. The numerical results in Table 3 demonstrate that the proposed approach is consistent with the reference solutions from [27], which were obtained using the RPT and IGA. The comparative results from Table 2 and Table 3 indicate that the modeling approach and the proposed methodology are appropriate for vibration analysis of sandwich plates with a metal foam core and CNTRC face sheets.

Table 2. *The first normalized frequency of the porous metal foam square plate (SSSS case, a/h = 5).*

Type	e_0	Mesh					Ref. [26]
		7×7	9×9	11×11	13×13	15×15	
P-I	0.3	0.2013	0.2013	0.2013	0.2013	0.2013	0.2008
	0.5	0.1918	0.1918	0.1918	0.1918	0.1918	0.1913
	0.7	0.1795	0.1795	0.1795	0.1795	0.1795	0.1790
P-II	0.3	0.2089	0.2089	0.2089	0.2089	0.2089	0.2084
	0.5	0.2067	0.2067	0.2067	0.2067	0.2067	0.2062
	0.7	0.2049	0.2049	0.2049	0.2049	0.2049	0.2039
P-III	0.3	0.2025	0.2025	0.2025	0.2025	0.2025	0.2020
	0.5	0.1936	0.1936	0.1936	0.1936	0.1936	0.1930
	0.7	0.1811	0.1811	0.1811	0.1811	0.1811	0.1840

Table 3. *The first four dimensionless natural frequencies of a metal foam plate for different porosity distributions and width to length ratios (e_0 = 0.2, a/h = 10).*

Type	Mode	BCs							
		SSSS				CCCC			
		b/a							
		1		2		1		2	
		Present	Ref. [27]	Present	Ref. [27]	Present	Ref. [27]	Present	Ref. [27]
P-I	1	5.6244	5.6244	3.5615	3.5615	9.6273	9.7136	6.7395	6.7810
	2	13.4007	13.4005	5.6246	5.6245	18.4157	18.748	8.6227	8.7355
	3	13.4007	13.4005	8.9536	8.9532	18.4157	18.748	11.9080	12.0742
	4	20.5422	18.6038	11.5224	11.5222	25.8762	26.4370	16.3067	16.5687
P-II	1	5.7905	5.7905	3.6704	3.6704	9.8612	9.9537	6.9146	6.9600
	2	13.7477	13.7475	5.7906	5.7906	18.7853	19.1415	8.8405	8.9638
	3	13.7477	13.7475	9.2034	9.2030	18.7853	19.1415	12.1946	12.3750
	4	21.0146	18.6313	11.8303	11.8301	26.3306	26.9222	16.6465	16.9312
P-III	1	5.6527	5.6527	3.5800	3.5800	9.6685	9.7558	6.7700	6.8121
	2	13.4610	13.4608	5.6529	5.6528	18.4832	18.8191	8.6609	8.7752
	3	13.4610	13.4608	8.9966	8.9962	18.4832	18.8191	11.9586	12.1269
	4	20.6258	18.6313	11.5757	11.5755	25.9614	26.5271	16.3683	16.6338

4.2. Parametric analysis

Table 4. *The influence CNTs distribution and porosity distribution on the first dimensionless frequency of the sandwich square plate (e_0 = 0.3, a/h = 10, h_c/h_f = 8).*

Type	CNTs	BCs					
		SSSS			CCCC		
		$\hat{V}_{CNT}$ = 0.11	$\hat{V}_{CNT}$ = 0.14	$\hat{V}_{CNT}$ =0.17	$\hat{V}_{CNT}$ = 0.11	$\hat{V}_{CNT}$ = 0.14	$\hat{V}_{CNT}$ = 0.17
P-I	FG-UD	4.6518	4.7195	4.7911	8.3280	8.4931	8.6549
	FG-UA	4.6704	4.7429	4.8192	8.3764	8.5534	8.7261
	FG-UO	4.6509	4.7183	4.7899	8.3251	8.4896	8.6511
	FG-UX	4.6529	4.7210	4.7930	8.3311	8.4971	8.6599
P-II	FG-UD	4.7596	4.8266	4.8976	8.4805	8.6427	8.8017
	FG-UA	4.7780	4.8499	4.9255	8.5285	8.7024	8.8722
	FG-UO	4.7586	4.8255	4.8964	8.4776	8.6392	8.7978
	FG-UX	4.7607	4.8281	4.8995	8.4836	8.6467	8.8067
P-III	FG-UD	4.6685	4.7363	4.8080	8.3542	8.5194	8.6813
	FG-UA	4.6871	4.7597	4.8361	8.4026	8.5796	8.7524
	FG-UO	4.6675	4.7351	4.8068	8.3513	8.5159	8.6774
	FG-UX	4.6696	4.7378	4.8099	8.3573	8.5234	8.6863

The free vibration response of the sandwich plates is conducted to deliver new computational results on the non-dimensional frequency $\bar{\Omega}$ of rectangular sandwich plates. The material properties of the carbon nanotube-reinforced face sheets are presented in Eq. (7), while the characteristics of the metal foam core are specified as E_1= 200 GPa, ν_1= 0.33, ρ_1= 7850 kg/m^3. Figure 4 presents the lowest normalized frequency of the sandwich plates under the influence of the porosity coefficient (e_0) and BCs. The results in Figure 4 show that, the CCCC sandwich plate exhibits the highest stiffness, whereas the SFSF sandwich plate has the lowest stiffness. Moreover, an increase in the coefficient e_0 corresponds to the reduction in the stiffness of the sandwich plate. The impact of porosity distribution and CNTs distribution pattern on the first normalized frequency of the sandwich plate is presented in Table 4. Based on the results in Table 4, the vibration frequency of the sandwich plate is significantly affected by the CNTs distribution pattern. In all cases, the highest frequency value is observed for the FG-UA distribution, while the FG-UO distribution yields the lowest frequency. The P-II porosity distribution of the core layer provides the highest frequency, followed by P-III and P-I porosity distributions. The influence of the length-to-width (a/b) and core-to-face thickness (h_c/h_f) ratios on the first natural frequency $\bar{\Omega}$ of the sandwich plate is investigated, and the results are presented in Table 5. When the ratio a/b decreases, the vibration frequency of the plate tends to increase. The higher the h_c/h_f ratio, the greater the vibration frequency.

Table 5. *The first normalized frequency of the sandwich rectangular plate with different porosity distributions, aspect ratios, and core-to-face thickness ratios (SSSS, e_0 = 0.1, FG-UD case, $\hat{V}_{CNT}$ = 0.11).*

h_c/h_f	a/b	*P-I*	*P-II*	*P-III*
4	1	4.2441	4.2541	4.2459
	1.5	2.8833	2.8896	2.8844
	2	2.4357	2.4408	2.4365
6	1	4.5840	4.6046	4.5877
	1.5	3.1966	3.2117	3.1992
	2	2.7295	2.7427	2.7318
8	1	4.8011	4.8302	4.8062
	1.5	3.3892	3.4111	3.3931
	2	2.9079	2.9270	2.9112
10	1	4.9499	4.9856	4.9563
	1.5	3.5190	3.5458	3.5237
	2	3.0273	3.0509	3.0315

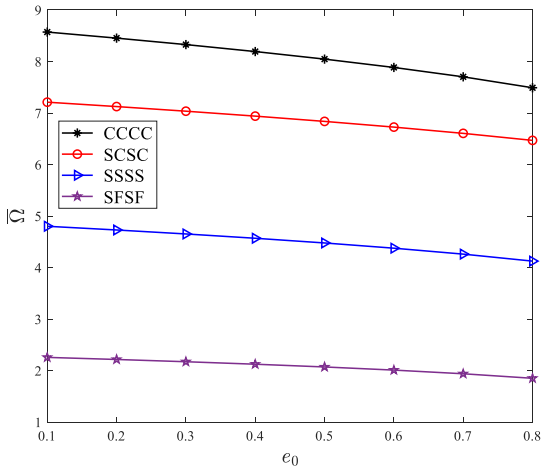

Figure 4. *The first dimensionless frequency of the sandwich plate for different porosity coefficients and BCs (P-I, FG-UD, $\hat{V}_{CNT}$ = 0.11, a/h = 10).*

5. Conclusions

This study performed free vibration of the sandwich plates incorporating a metal foam core and two face sheets reinforced with CNTs using HSDT and the IGA. The results offer insights regarding various factors influencing the dynamic characteristics of the sandwich plate, specifically as follows:

- The numerical results obtained exhibit high accuracy, aligning well with previous methods and references, thereby confirming the reliability of the applied approach.
- The increase in the porosity coefficient leads to a decrease in the natural frequency of the sandwich plate.
- The CCCC plate provides the highest stiffness, while the SFSF plate condition results in the lowest stiffness.
- Among the CNTs distribution types, the FG-UA pattern gives the highest natural frequency, whereas the FG-UO pattern results in the lowest natural frequency.
- Increasing the length-to-width ratio reduces the natural frequency and decreases the stiffness of the plate.

Conflict of Interest

The authors declare no conflict of interest.

REFERENCES

[1] D. Chen, S. Kitipornchai, and J. J. Yang, "Nonlinear free vibration of shear deformable sandwich beam with a functionally graded porous core," *Thin-Walled Structures*, vol. 107, pp. 39–48, 2016.
[2] Y. Q. Wang and H. L. Zhao, "Free vibration analysis of metal foam core sandwich beams on elastic foundation using Chebyshev collocation method," *Archive of Applied Mechanics*, vol. 89, pp. 2335–2349, 2019.
[3] M. R. Barati, H. Shahverdi, and A. M. Zenkour, "Electro-mechanical vibration of smart piezoelectric FG plates with porosities according to a refined four-variable theory," *Mechanics of Advanced Materials and Structures*, vol. 24, no. 12, pp. 987–998, 2017.
[4] N. Wattanasakulpong and A. Chaikittiratana, "Flexural vibration of imperfect functionally graded beams based on Timoshenko beam theory: Chebyshev collocation method," *Meccanica*, vol. 50, pp. 1331–1342, 2015.
[5] F. Ebrahimi, A. Jafari, and M. R. Barati, "Free vibration analysis of smart porous plates subjected to various physical fields considering neutral surface position," *Arabian Journal for Science and Engineering*, vol. 42, no. 5, pp. 1865–1881, 2017.
[6] Y. Q. Wang and Z. Y. Zhang, "Bending and buckling of three-dimensional graphene foam plates," *Results in Physics*, vol. 13, p. 102136, 2019.
[7] A. Mojahedin, M. Jabbari, A. Khorshidvand, and M. Eslami, "Buckling analysis of functionally graded circular plates made of saturated porous materials based on higher order shear deformation theory," *Thin-Walled Structures*, vol. 99, pp. 83–90, 2016.
[8] Z. Lei, L. Zhang, and K. B. Liew, "Vibration of FG-CNT reinforced composite thick quadrilateral plates resting on Pasternak foundations," *Engineering Analysis with Boundary Elements*, vol. 64, pp. 1–11, 2016.
[9] L. Zhang, Z. Song, and K. C. Liew, "State-space Levy method for vibration analysis of FG-CNT composite plates subjected to in-plane loads based on higher-order shear deformation theory," *Composite Structures*, vol. 134, pp. 989–1003, 2015.
[10] P. Jiao, Z. Chen, Y. Li, H. Ma, and J. Wu, "Dynamic buckling analyses of functionally graded carbon nanotubes reinforced composite (FG-CNTRC) cylindrical shell under axial power-law time-varying displacement load," *Composite Structures*, vol. 220, pp. 784–797, 2019.
[11] T. J. Hughes, J. A. Cottrell, and Y. Bazilevs, "Isogeometric analysis: CAD, finite elements, NURBS, exact geometry and mesh refinement," *Computer Methods in Applied Mechanics and Engineering*, vol. 194, no. 39–41, pp. 4135–4195, 2005.
[12] Z. Kacprzyk and K. Ostapska-Łuczkowska, "Isogeometric analysis as a new FEM formulation—Simple problems of steady-state thermal analysis," *Procedia Engineering*, vol. 91, pp. 87–92, 2014.
[13] T. A. Huynh, A. T. Luu, and J. J. Lee, "Bending, buckling and free vibration analyses of functionally graded curved beams with variable curvatures using isogeometric approach," *Meccanica*, vol. 52, pp. 2527–2546, 2017.
[14] C. H. Thai, H. Nguyen-Xuan, S. P. A. Bordas, N. Nguyen-Thanh, and T. Rabczuk, "Isogeometric analysis of laminated composite plates using the higher-order shear deformation theory," *Mechanics of Advanced Materials and Structures*, vol. 22, no. 6, pp. 451–469, 2015.
[15] M. R. Barati, "Nonlocal-strain gradient forced vibration analysis of metal foam nanoplates with uniform and graded porosities," *Advances in Nano Research*, vol. 5, no. 4, pp. 393–402, 2017.
[16] H. S. Shen, "Postbuckling of nanotube-reinforced composite cylindrical shells in thermal environments, Part I: Axially loaded shells," *Composite Structures*, vol. 93, no. 8, pp. 2096–2108, 2011.
[17] J. Jam and Y. Kiani, "Buckling of pressurized functionally graded carbon nanotube reinforced conical shells," *Composite Structures*, vol. 125, pp. 586–595, 2015.
[18] M. Mirzaei and Y. Kiani, "Thermal buckling of temperature-dependent FG-CNT reinforced composite plates," *Meccanica*, vol. 51, pp. 2185–2201, 2016.
[19] Y. Kiani, "Thermal postbuckling of temperature-dependent sandwich beams with carbon nanotube-reinforced face sheets," *Journal of Thermal Stresses*, vol. 39, no. 9, pp. 1098–1110, 2016.
[20] H. S. Shen, "Nonlinear bending of functionally graded carbon nanotube-reinforced composite plates in thermal environments," *Composite Structures*, vol. 91, no. 1, pp. 9–19, 2009.
[21] Z. X. Wang and H. S. Shen, "Nonlinear vibration of nanotube-reinforced composite plates in thermal environments," *Computational Materials Science*, vol. 50, no. 8, pp. 2319–2330, 2011.
[22] Z. X. Wang and H. S. Shen, "Nonlinear vibration and bending of sandwich plates with nanotube-reinforced composite face sheets," *Composites Part B: Engineering*, vol. 43, no. 2, pp. 411–421, 2012.

[23] Z. X. Wang, J. Xu, and P. Qiao, "Nonlinear low-velocity impact analysis of temperature-dependent nanotube-reinforced composite plates," *Composite Structures*, vol. 108, pp. 423–434, 2014.
[24] J. N. Reddy, "A simple higher-order theory for laminated composite plates," *Journal of Applied Mechanics*, vol. 51, no. 4, pp. 745–752, 1984.
[25] H. Nguyen-Xuan, C. H. Thai, and T. Nguyen-Thoi, "Isogeometric finite element analysis of composite sandwich plates using a higher order shear deformation theory," *Composites Part B: Engineering*, vol. 55, pp. 558–574, 2013.
[26] M. Heshmati and F. Daneshmand, "A study on the vibrational properties of weight-efficient plates made of material with functionally graded porosity," *Composite Structures*, vol. 200, pp. 229–238, 2018.
[27] H. Pham-Tan, C. H. Thai, and P. Phung-Van, "NURBS-based refined plate theory for metal foam plates with porosities," *Thin-Walled Structures*, vol. 175, p. 109246, 2022.

Duy-Khang Pham was born in Vietnam in 2000. In 2023, he graduated with a Bachelor's degree in Civil Engineering from Ho Chi Minh City University of Technology and Education. He is currently pursuing a Master's degree in Mechanics at the same university. His research interest is computational mechanics.
Email address: pduykhang18@gmail.com. ORCID: https://orcid.org/0009-0005-2486-5898

Minh-Tan Huynh is from Ho Chi Minh City, Vietnam, born in 1997. He is a civil engineer who graduated in 2020 from Thu Dau Mot University. Currently, he is pursuing a master's degree at Ho Chi Minh City University of Technology and Education. His research interest is computational mechanics.
Email address: tan.mh287@gmail.com. ORCID: https://orcid.org/0009-0001-1698-5073

Tan-Hung Pham was born in Vietnam in 1981. He has a Ph.D. degree in Mechanics. Now, he is a lecturer at the Faculty of Civil Engineering at Ho Chi Minh City University of Technology and Education, Ho Chi Minh City, Vietnam. His research interests are the computational mechanics.
Email address: hungpht@hcmute.edu.vn. ORCID: https://orcid.org/0000-0001-6105-9311